Letter

Chiral broken symmetry descendants of the kagome lattice chiral spin liquid

Anjishnu Bose,[1] Arijit Haldar,[1] Erik S. Sørensen,[2] and Arun Paramekanti[1,*]
[1]*Department of Physics, University of Toronto, 60 St. George Street, Toronto, Ontario, Canada M5S 1A7*
[2]*Department of Physics, McMaster University, 1280 Main St. W., Hamilton, Ontario, Canada L8S 4M1*

(Received 3 May 2022; accepted 11 January 2023; published 25 January 2023)

The breaking of chiral and time-reversal symmetries provides a pathway to exotic quantum phenomena and topological phases. Recent work has extensively explored the resulting emergence of chiral charge orders and chiral spin liquids (CSLs) on the kagome lattice. Such CSLs are closely tied to bosonic fractional quantum Hall states with anyonic quasiparticles; however, their connection to nearby ordered states has remained a mystery. Here, we use spin-wave theory, parton Gutzwiller wave functions, and exact diagonalization to show that two distinct magnetic orders with uniform scalar chirality—the XYZ umbrella state and the octahedral spin crystal–emerge as competing orders in close proximity to the CSL. In this letter, we highlight the intimate link between a topologically ordered liquid and broken symmetry states with nontrivial real-space topology.

DOI: 10.1103/PhysRevB.107.L020411

Introduction. Quantum spin liquids (QSLs) are strongly entangled phases of quantum magnets which exhibit exotic quasiparticle excitations [1–4]. The classic work of Kalmeyer and Laughlin [5] revealed a direct relation between a class of such QSLs, with broken mirror and time-reversal symmetries, and gapped fractional quantum Hall states of bosons with anyon excitations. Important progress was later made in identifying microscopic models on different lattices for which such chiral spin liquids (CSLs) are exact [6–8] or numerically tractable [9–17] ground states. A valuable development was the identification of the Kalmeyer-Laughlin liquid in an SU(2) invariant model with a simple three-spin scalar chiral exchange coupling on the geometrically frustrated kagome lattice [10–13], a network of corner-sharing triangles reminiscent of a Japanese woven basket [18]. While the nearest-neighbor kagome lattice Heisenberg model has been argued to host a Dirac spin liquid [19–23], the inclusion of longer-range couplings has been shown to realize CSLs [11–13,24] arising from spontaneous breaking of mirror and time-reversal symmetries. A variety of these competing phases have been proposed to occur in materials such as Herbertsmithite [25,26] and Zn-barlowite [27]. Optical driving [28], proximity to Mott transitions [16], and twisted moiré crystals [29] are potential experimental routes to obtain CSLs and even topological superconductors upon doping [30,31]. More recently, Rydberg atom quantum simulators have shown the promise to access such topological spin liquids [32].

In parallel with the interest in such CSLs, there has been great interest in chiral broken symmetry states in geometrically frustrated systems, which can potentially display nontrivial real-space topology, giving rise to the nascent field of chiraltronics. The most well-known examples of these are skyrmion and meron crystals—creating and manipulating such topological textures has important spintronics and information storage applications [33–38]. More recently, chiral density-wave orders have been reported in the metallic kagome materials AV_3Sb_5 [39–43], and chiral magnetic orders have been explored in FeGe [44]. How are the topologically ordered states such as CSLs related to chiral broken symmetry states with nontrivial real-space topology? Historically, there was an attempt to relate the fractional quantum Hall liquid to a melted Wigner crystal of electrons driven by multiparticle exchanges [45]. The analogous question in the field of QSLs is to ask how they arise from the melting of parent magnetically ordered states. For instance, gapped Z_2 QSLs descend from quantum melting of coplanar magnetic orders while preserving pointlike topological Z_2 vortex defects [46]. Previous exact diagonalization (ED) and density-matrix renormalization group (DMRG) calculations have found CSLs and tetrahedral spin crystals on triangular and honeycomb lattices [9,15,17,47] and complex noncoplanar orders in kagome lattices with staggered chiral terms which hosts a gapless CSL [48]. Here, we show that the kagome lattice CSL is in close proximity to two distinct symmetry-breaking orders which feature a uniform nonzero scalar spin chirality, a nontrivial real-space topological feature they partially share with skyrmion crystals [33,34]. The scalar chirality is a source of Berry fluxes, which can transmute to background gauge fluxes in an effective gauge theory description of the spin-$\frac{1}{2}$ CSL [14,49–51]. Our work links a many-body topologically ordered state to the quantum melting of proximate chiral broken symmetry states with nontrivial real-space topology and shows how both of these ultimately emerge from a highly degenerate manifold of classical chiral states.

Model Hamiltonian and Classical Orders. We consider the kagome lattice model Hamiltonian:

$$H_{\rm spin} = -J_\chi \sum_{\triangle,\triangledown} \mathbf{S}_i \cdot \mathbf{S}_j \times \mathbf{S}_k + J_3 \sum_{\hexagon} \mathbf{S}_i \cdot \mathbf{S}_j. \quad (1)$$

Figure 1(a) shows the chiral three-spin interaction J_χ acting on triangular plaquettes (with spins $[ijk]$ ordered anticlockwise), and the J_3 Heisenberg term coupling farther spins on kagome

*arunp@physics.utoronto.ca

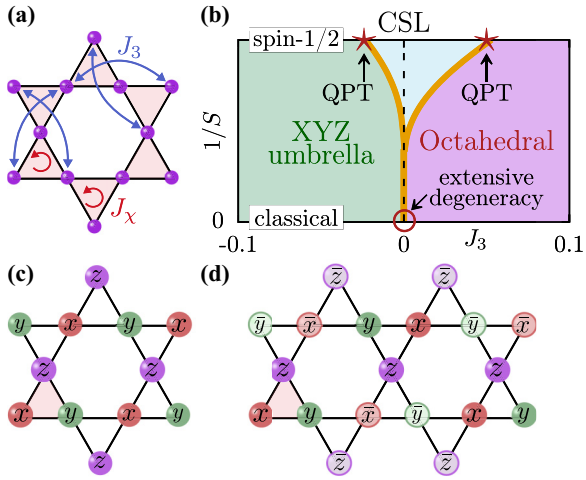

FIG. 1. Kagome lattice. (a) The chiral three-spin interactions and further neighbor two-spin couplings in the model H_{spin}. (b) Proposed phase diagram of the model H_{spin} as we tune J_3 and the strength of quantum fluctuations via $1/S$ where S is the spin length. For spin $S = \frac{1}{2}$, the extensively degenerate classical point evolves into an emergent chiral spin liquid, bounded by noncoplanar magnetic orders. The light blue region indicates where spin-wave fluctuations can destabilize the noncoplanar orders, hinting at a quantum spin liquid. (c) The classical limit XYZ ordering pattern, indicating spins pointing along x, y, z. The XYZ umbrella order has the same symmetries as the classical XYZ order but has an opening angle between the three spins on the triangle which lies between the orthogonal XYZ triad and coplanar 120° order. (d) Octahedral magnetic order with quadrupled unit cell and spins pointing along $(x, \bar{x})$, $(y, \bar{y})$, $(z, \bar{z})$, where $\bar{x} \equiv -x$.

bow ties. Without loss of generality, we fix $J_\chi = 1$. Our proposed phase diagram for this model is depicted in Fig. 1(b), as we tune J_3 and the spin length S which controls the degree of quantum fluctuations. It prominently features two distinct chiral broken symmetry orders and the CSL in the spin-$\frac{1}{2}$ limit.

When $J_3 = 0$ in Eq. (1), minimizing the energy amounts to maximizing the scalar spin chirality. In the classical limit, where we treat spins as classical unit vectors, this implies that each triangle has spins which must form an orthonormal triad, e.g., going anticlockwise around a triangle, we may have spins pointing along $\{x, y, z\}$. As shown in recent work on the kagome lattice [52], there can be many choices for how to place these triads on adjacent triangles, so that the number of classical ground states scales as $\Omega \sim 2^{N/3}$, where N is the number of kagome sites.

However, we see that any nonzero $J_3 < 0$ completely breaks this degeneracy, selecting a ground state with XYZ order, as shown in Fig. 1(c). This XYZ state is a specific member of the family of $\mathbf{Q} = 0$ umbrella states which have the same unit cell as the original kagome lattice; see Supplemental Material (SM) [53]. In the opposite limit, when $J_\chi = 0$, the kagome lattice decouples into three rhombic sublattices, each of which individually supports ferromagnetic order driven by $J_3 < 0$. In this limit, introducing an infinitesimal J_χ couples the three sublattices, again leading to XYZ order. The XYZ state can thus be shown to be the unique classical ground state of H for any $J_3 < 0$ since it separately minimizes each term in the Hamiltonian. A similar analysis indicates that $J_3 > 0$ leads to antiferromagnetically coupled rhombic sublattices. This selects octahedral order shown in Fig. 1(d) (see also SM [53]), with a 12-site unit cell and zero net magnetization, as the unique classical ground state. Spins in the XYZ state subtend a solid angle $\pi/2$ over elementary triangular plaquettes and trace out $-\pi$ over hexagons. With octahedral order, spins subtend a solid angle $\pi/2$ over triangular plaquettes and trace out $+\pi$ over hexagons; it may be viewed as a dense crystal of baby skyrmions. The XYZ and octahedral states are regular magnetic orders [54], where lattice symmetries are only broken due to broken spin rotation symmetries; restoring spin rotation symmetry via quantum fluctuations is thus expected to result in symmetric QSLs.

Quantum Fluctuations. Leading-order quantum fluctuations in spin models may be treated using linear spin wave theory (SWT) which is exact to $O(1/S)$. To formally treat our model Hamiltonian within SWT, we rescale $J_\chi \to J_\chi/(2S)$ in Eq. (1), which leaves the spin-$\frac{1}{2}$ model unchanged but allows the two- and three-spin terms to compete in the $S \to \infty$ limit. We then treat the small fluctuations around the XYZ and octahedral orders by deriving and solving the bosonic Bogoliubov–de Gennes SWT Hamiltonian directly in real space; see Supplemental Material (SM) [53]. Using this approach, we find that the octahedral state spectrum admits three exact zero modes, consistent with the expected number of Nambu-Goldstone modes of the fully broken spin rotational symmetry, while the XYZ order admits two zero modes due to the nonzero net magnetization [55]. As $J_3 \to 0$, many spin-wave modes descend and merge with the zero modes, reflecting the extensive degeneracy of the classical ground states at $J_3 = 0$ [52].

Dropping the exact zero modes on finite-sized systems, we have computed the SWT correction to the classical octahedral and XYZ order parameters and extrapolated the result to the thermodynamic limit [53]. We respectively denote these as $M_\pm$ for $J_3 > 0$ and $J_3 < 0$. These order parameters take the form $M_\pm = S - \alpha_\pm(J_3)$, where the correction term $\alpha_\pm$ depends on J_3 but is independent of S. For small values of $|J_3|$, these are well fit by the expressions $\alpha_\pm(J_3) = c_\pm \ln(1/|J3|)$, where $c_+ \approx 0.068$ and $c_- \approx 0.053$; this logarithmic divergence as $J_3 \to 0^\pm$ is consistent with the absence of long-range order at $J_3 = 0$.

We identify the critical spin value S_c where these noncoplanar orders melt for a given J_3 using an analog of the well-known Lindemann criterion for melting of crystals. For the magnetic order to melt, we demand that $\alpha_\pm(J_3) > fS$, where f is a constant. This is equivalent to demanding that the fluctuations exceed a sizable fraction of the classical ordered moment. Using this, we obtain $1/S_c^{(\pm)} = (f/c_\pm)/\ln(1/|J_3|)$. For $f = 0.4$, we find for spin $S = \frac{1}{2}$ that this leads to loss of octahedral order for $0 < J_3 \lesssim 0.05$ and a breakdown of the XYZ order in the regime $-0.02 \lesssim J_3 < 0$. In the $S = \frac{1}{2}$ model, we will see below that this (approximate) window around $J_3 = 0$ gets replaced by the CSL. Plotting the melting curve for all S leads to the phase boundaries marked in Fig. 1(b), which reveals a spin-liquid fan emanating from the extensively degenerate classical chiral point.

Parton Mean-Field Theory. To study the phase diagram of this model in the quantum limit of $S = \frac{1}{2}$, we begin with a Schwinger fermion representation of the spin $\mathbf{S}_i = f^\dagger_{i\alpha}\boldsymbol{\sigma}_{\alpha\beta}f_{i\beta}/2$, with an implicit sum on repeated (Greek) spin indices. Previous DMRG and ED calculations [10] on the pure chiral model with $J_3 = 0$ have shown that it supports a Kalmeyer-Laughlin CSL ground state. At mean-field level, this CSL may be described as a topological band insulator of f partons, with total Chern number $C = 2$ [49]. To study the impact of small J_3, we recast the spin model in terms of partons:

$$H_{\rm p} = \sum_{ij} t_{ij} f^\dagger_{i\alpha} f_{j\alpha} + \frac{J_3}{4} \sum_{\hexagon\!\!\!\!\hexagon} f^\dagger_{i\alpha}\sigma_{\alpha\beta}f_{i\beta} \cdot f^\dagger_{j\mu}\sigma_{\mu\nu}f_{j\nu}. \quad (2)$$

Here, the first term is a kagome Hofstadter model which captures the mean-field description of the CSL at $J_3 = 0$ [19,56]. The complex hoppings t_{ij} are fixed to have equal magnitude $|t_{ij}| = t$ on all nearest-neighbor bonds and phases chosen such that the partons experience $\pi/2$-flux around elementary triangular plaquettes and zero-flux around hexagonal plaquettes. This supports Chern bands with total Chern number $C = 2$ (counting both spin-↑ and spin-↓) at half-filling, providing the correct starting point for the low-energy $U(1)_2$ Chern-Simons gauge theory description of the CSL [49]. The mean-field spin gap in this insulator is equal to its insulating band gap $\Delta_{mf} \approx 1.46t$. Matching this to the ED result for the spin gap $\Delta \approx 0.05J_\chi$ of the pure chiral model (see Ref. [10] and Fig. 4 below) fixes $t = 0.034J_\chi$. The second term in Eq. (2) is obtained by rewriting the J_3 spin interaction in Eq. (1) in terms of partons. This Hamiltonian supplemented by a mean-field constraint $\langle f^\dagger_{i\alpha} f_{i\alpha}\rangle = 1$ at each site.

To examine the impact of nonzero J_3, we treat the four-fermion terms using a spatially inhomogeneous and unbiased mean-field theory, with an independent Weiss field on every site, and allowing for complex hoppings across the bow ties of the kagome (i.e., sites connected by J_3). We then perform a variational mean-field theory analysis on system sizes up to 108 sites [53]. We find that the complex hopping across the bow ties ends up being vanishingly small at the global variational minimum and hence can be safely ignored. For small $|J_3|$, the gapped Chern insulator is stable to four-fermion interactions. Beyond a critical coupling, the internal Weiss fields become nonzero, with a uniform strength $\mathcal{B}$ and directions which are spatially modulated, signifying magnetic symmetry breaking. For $J_3 > 0.092J_\chi$, we find that the converged broken symmetry pattern shows a clear pattern of octahedral order with a reconstructed 12-site unit cell (2×2 kagome unit cell). For $J_3 < -0.077J_\chi$, the solution converges to XYZ umbrella order, i.e., an umbrella state which shares all symmetries of the XYZ order, but is intermediate between the XYZ state and the $\mathbf{Q} = 0$ coplanar 120° state. [Given that $H_{\rm p}$ in Eq. (2) builds upon the mean-field CSL state at $J_3 = 0$, the parton results are only valid for $J_3/J_\chi \ll 1$.] The resulting phase diagram is shown in Fig. 2, including the total Chern number of the occupied bands [57] as we tune J_3 [53]. Beyond mean-field theory, the broken symmetry insulators are expected to have trivial many-body topology.

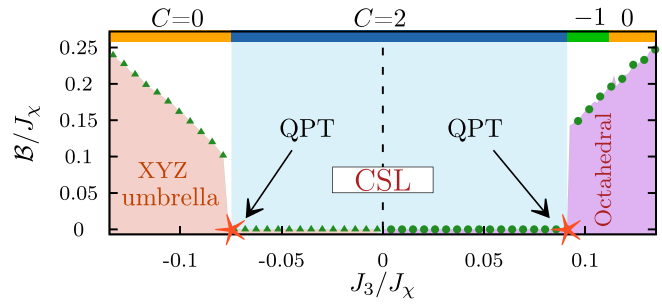

FIG. 2. Parton theory phase diagram. Mean-field phase diagram of the $S = \frac{1}{2}$ parton theory of Eq. (2) as we vary J_3/J_χ. For $J_3 > 0.092J_\chi$, we find a phase transition from the mean-field chiral spin liquid (CSL) into the octahedral state, while for $J_3 < -0.077J_\chi$, we find an instability into the XYZ umbrella order, a state with the same symmetries as the XYZ state. The top line depicts the total Chern number of the half-filled parton bands in various phases as we tune J_3/J_χ.

Gutzwiller Projected Wave Functions. To go beyond parton mean-field theory and strictly implement the Gutzwiller projection constraint (i.e., exactly one fermion per site), we next turn to a Monte Carlo study of the projected parton wave function [58] to optimize its parameters and study its properties. We consider a parton state $|\Psi_f\rangle$ which is obtained as the Slater determinant ground state of a variational Hamiltonian which includes complex nearest-neighbor hopping $e^{i\theta_{ij}}$ and next-neighbor hopping $\gamma e^{i\phi_{ij}}$ [58], with phases chosen to enclose uniform fluxes Θ, Φ through elementary and large triangular plaquettes, as in Fig. 3(a). To account for magnetic symmetry-breaking orders, we include variational Weiss fields $\mathbf{b}_i$ via $-\sum_i \mathbf{b}_i \cdot f^\dagger_{i\alpha}\boldsymbol{\sigma}_{\alpha\beta}f_{i\beta}/2$, limiting ourselves to $J_3 > 0$ octahedral order; the $\mathbf{b}_i$ are thus chosen to have an octahedral pattern, as indicated in Fig. 3(a), as motivated by our classical and parton mean-field theory results, with a spatially uniform magnitude $|\mathbf{b}_i| = \mathcal{B}_{\rm oct}$. We explore the variational ansatz $|\Psi_G\rangle = \prod_{\hexagon} \exp\{-g\,(S^z[\hexagon])^2\}\; P_G|\Psi_f\rangle$, where P_G denotes Gutzwiller projection to one electron per site. The Gutzwiller wave function $P_G|\Psi_f\rangle$ is supplemented with a product Jastrow correlation factor acting on every kagome bow tie, as shown in Fig. 3(a), where g is the strength of the Jastrow factor, and $S^z[\;\hexagon\;]$ denotes the total S^z on the bow tie excluding the central site. The set of variational parameters explored in our study are $\{\gamma, \Theta, \Phi, g, \mathcal{B}_{\rm oct}\}$ [53]. (We have checked that an optimized variational third-neighbor hopping across sites connected by J_3 is negligible; the main effect of J_3 is to induce symmetry-breaking Weiss fields.)

For small J_3/J_χ of interest, we obtain reasonable variational energies by fixing $\Theta = \pi/2$ and $\gamma = 0.2$ and setting the Jastrow strength to $g = 0.045$. We then vary $\Phi, \mathcal{B}_{\rm oct}$ to explore the variational space for different values of J_3 (with $J_\chi = 1$). For the pure chiral model ($J_3 = 0$), our wave function on an 8×8 kagome lattice (192 spins) yields an energy per site $\simeq -0.151(1)J_\chi$; this is somewhat higher than ED ($\approx -0.1729J_\chi$, $N = 36$) and an infinite projected entangled-pair state study [59] which yielded $\approx -0.1715J_\chi$. Figure 3(b) shows the variational energy as a function of $\mathcal{B}_{\rm oct}$ for various values of J_3, where we have optimized with respect to Φ at each point. For $J_3 = 0$, we find that the CSL is stable

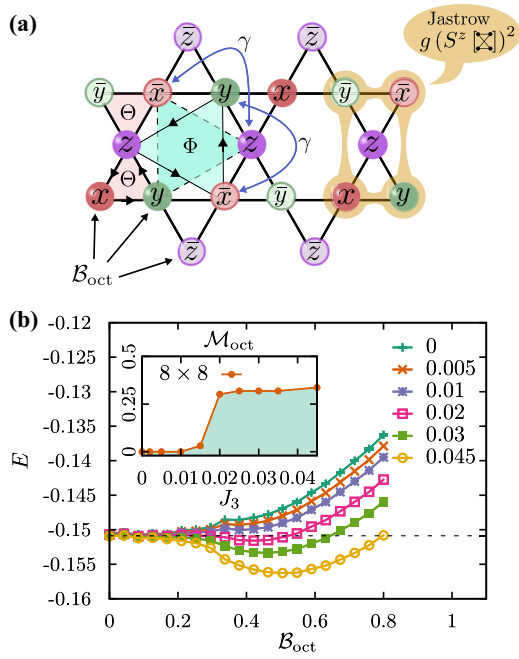

FIG. 3. Gutzwiller wave function study. (a) Variational parameters used in our kagome wave function ansatz include a second-neighbor hopping of strength γ, fluxes Θ, Φ through elementary and large triangular plaquettes (shaded), a local Jastrow factor which suppresses the total S^z on bow ties (excluding the central site), and a Weiss field $\mathcal{B}_{\rm oct}$ which induces octahedral order; field directions are depicted on the sites. (b) Variational energy vs $\mathcal{B}_{\rm oct}$ for an 8×8 lattice for different J_3, showing a stable chiral spin liquid (CSL) state for $J_3 = 0$ and an instability to octahedral order for $J_3 \gtrsim 0.02$. The inset shows the order parameter $\mathcal{M}_{\rm oct}$ which becomes nonzero in the ordered phase.

toward octahedral order but with an apparent metastable minimum at nonzero $\mathcal{B}_{\rm tot}$. With increasing J_3, this metastable minimum rapidly comes down in energy, becoming the true minimum for $J_3/J_\chi \gtrsim 0.02$, signalling a first-order transition into the octahedral state. As shown in the inset to Fig. 3(b), the octahedral order parameter $\mathcal{M}_{\rm oct} = (1/N)\sum_i \mathbf{m}_i \cdot \hat{\mathbf{b}}_i$ jumps at this transition. A better CSL wave function at $J_3 = 0$ will have lower energy, rendering the CSL more stable and increasing the critical value of J_3 for the octahedral instability.

Exact Diagonalization Results. ED is a powerful unbiased tool to study frustrated kagome quantum magnets [10,60–62]. To corroborate our results from the preceding sections, we have carried out ED calculations for the spin Hamiltonian in Eq. (1) on various finite-sized kagome clusters, ranging in size from $N = 12$ to 36 (shown in SM [53]). The largest clusters are studied using a fully parallelized Lanczos code that is most optimally used only with the total S^z_T as a quantum number [63]. A full symmetry analysis can be performed on the smaller clusters (see SM [53]). Our results for the spin gaps to the lowest-lying states in each S^z_T sector are shown in Fig. 4(a) vs J_3. Two transitions are visible, indicated by the shaded red regions. For $J_3 \lesssim J^c_{\rm XYZ} \approx -0.03 J_\chi$, the ground state transitions away from a singlet [64], and the system becomes ferromagnetic, consistent with the appearance of the XYZ umbrella state. In the vicinity of $J_3 = J^c_{\rm oct} \approx 0.06 J_\chi$, the spin gap appears to close, signaling a second-order transition within ED [65] to a different state. These values of J^c_3 compare favorably with the estimates obtained in our previous analysis. In the CSL regime for $J^c_{\rm XYZ} < J_3 < J^c_{\rm oct}$, our results are consistent with a finite spin gap to the first $S = 1$ state above two $S = 0$ states.

To identify the magnetically ordered states adjoining the CSL phase, we apply a finite $h_{\rm XYZ}$ and $h_{\rm oct}$ to a single triangle [shown in shaded red in Figs. 4(b) and 4(c)] for the largest $N = 36$ cluster and study the induced ordering at the other sites. This applied field breaks all Hamiltonian symmetries, necessitating a diagonalization in the full 2^{36}-dimensional Hilbert space. The results are shown in Figs. 4(b) and 4(c) for $h_{\rm XYZ}, h_{\rm oct} = 0.4$ at $J_3 = -0.5$ and $J_3 = 0.15$, respectively. The observed patterns are clearly consistent with the XYZ umbrella and octahedral ordering, with only limited decrease in the overlap as one moves away from the triangle where the field is applied (shaded red). We calculate the induced $\mathcal{M}_{\rm oct} = 0.311$ at $J_3 = 0.15 J_\chi$, in good agreement with the Gutzwiller wave function result, and $\mathcal{M}_{\rm XYZ} = 0.443$ at $J_3 = -0.5 J_\chi$. Our ED results unequivocally point to the presence of octahedral and XYZ umbrella orders adjacent to the CSL.

For $J_3 < 0$, the destabilization of the CSL first occurs via a higher spin state becoming the ground state; this occurs at $J_3/J_\chi \approx -0.04$ for $N = 12$ (see SM [53]) as well as $N = 24$ (see Fig. 4). However, we can also identify a

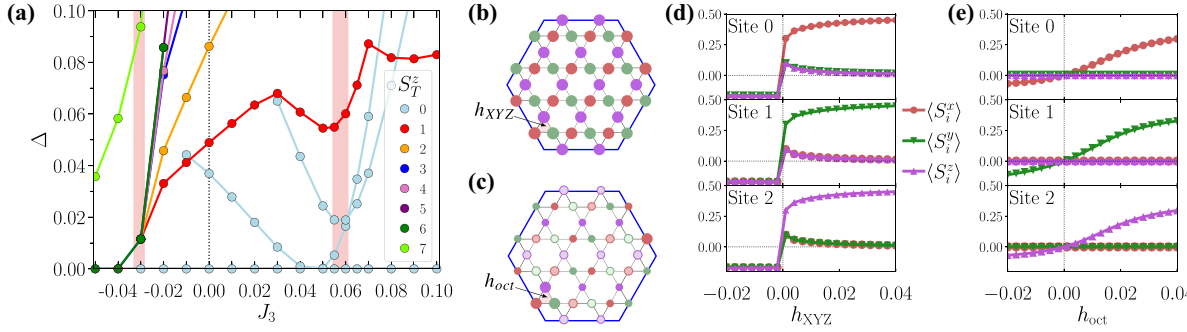

FIG. 4. Exact diagonalization results. (a) Gaps to the lowest-lying $S^z_T = 0, \ldots 7$ states for the 36-site cluster. (b) The induced $\langle S^\alpha\rangle$ for the 36-site cluster with a Zeeman field $h_{\rm XYZ}$ applied to a single triangle (shaded) at $J_3 = -0.5$, and (c) with a $h_{\rm oct}$ applied to a single triangle (shaded) at $J_3 = 0.1$. The radius of the points are proportional to the overlap with the expected XYZ or octahedral ordering direction at each site. (d) $\langle S^\alpha\rangle$ on adjacent sites taken anticlockwise on any given single up triangle for the 24*Rh*-site cluster in a uniform $h_{\rm XYZ}$ field with $J_3 = -1.4$. (e) $\langle S^\alpha\rangle$ on adjacent sites on a single triangle for the 24-site cluster in a uniform $h_{\rm oct}$ field with $J_3 = 0.15$.

second transition in the spectrum at even higher $|J_3|$ where a maximal spin ground state is achieved—this appears to signal that the CSL first undergoes a transition into an XYZ umbrella state which then reaches an endpoint where it transitions into perfect XYZ order. However, this second transition point shifts significantly with system size: from $J_3/J_\chi \approx -0.15$ for $N = 12$ (with $S_{\max} = 3$) to $J_3/J_\chi \approx -1.13$ for $N = 24$ (with $S_{\max} = 7$); see SM [53]. It is thus plausible that, with increasing N, the XYZ umbrella order only becomes the perfectly orthogonal XYZ state for $|J_3|/J_\chi \to \infty$.

To further study the induced orders for $J_3 < 0$, we apply a Zeeman field of the form $-\sum_\triangle h^\alpha_{\mathrm{XYZ}} S^\alpha$ uniformly on all up triangles in the lattice, so that each kagome site is counted once. We then measure the response on a single up triangle with sites numbered (0, 1, 2) in anticlockwise order. For $J_3 < 0$, such a field term will induce the XYZ umbrella state at large h_{XYZ}. The response $\langle S^\alpha \rangle$ vs h_{XYZ} on the three sites 0, 1, and 2 is shown in Fig. 4(d) at $J_3 = -1.4 J_\chi$ for the $24Rh$ cluster. Due to the degenerate ground state at $J_3 = -1.4 J_\chi$, a discontinuous jump in all $\langle S^\alpha \rangle$ is observed at $h_{\mathrm{XYZ}} = 0$, resulting in a divergent susceptibility with respect to the XYZ umbrella state. In a similar manner, for $J_3 > 0$, we can apply a field term of the form $-\sum_\triangle h^\alpha_{\mathrm{oct}} S^\alpha$ with h^α_{oct} now reflecting the octahedral ordering shown in Fig. 1(c), with a pattern like the Weiss field $\mathcal{B}_{\mathrm{oct}}$ used in our variational study. The response of the system to such a field on the sites 0, 1, and 2 is shown in Fig. 4(e) vs h_{oct} at $J_3 = 0.15 J_\chi$ for the 24 clusters. (The octahedral ordering is not compatible with the $24Rh$ cluster). Because of the nonzero spin gap, the response is more gradual, but $\langle S^\alpha \rangle$ quickly reach values close to saturation even for small fields. For this value of J_3, we expect the spin gap to close with increasing system size N. In the limit $h_{\mathrm{oct}} \to 0$, we interpret $\partial \langle S^\alpha \rangle / \partial h_{\mathrm{oct}}$ as a susceptibility to octahedral ordering; we have verified that this susceptibility appears to diverge with increasing N [53]. On the other hand, if h_{XYZ} or h_{oct} is applied within the CSL, a first-order transition to an ordered state is observed at a finite value of the field [53].

Conclusions. In this letter, we have used SWT, ED, and Gutzwiller wave functions to uncover two chiral magnetic orders—XYZ order and octahedral order—near the gapped CSL on the kagome lattice, which are accessed by tuning a small Heisenberg interaction across the bow ties. Our proposed global phase diagram, as we vary spin S, hints at the possibility of unusual QSLs in the chiral model for higher spin, including spin-1 magnets, opening up a promising research direction. Our work unveils distinct noncoplanar orders on the kagome lattice with uniform spin chirality and points to a tantalizing universal connection between many-body topological order in the gapped CSL and real-space topology encoded in Berry fluxes of the noncoplanar broken symmetries. While our parton mean-field theory and variational Monte Carlo calculations find a first-order transition from the CSL into the XYZ or octahedral states, our ED results, which we expect to be more reliable than the variational wave function calculations, are instead suggestive of a possibly continuous gap closing transition for $J_3 > 0$. Further research is needed to explore this possibility; we emphasize that we do not, at present, have a field theory description of this CSL-octahedral transition. In addition, for $J_3 < 0$, it would be desirable to construct a variational spin-wave approach which would allow us to better understand the evolution of the XYZ umbrella into the perfect XYZ state with increasing $|J_3|$. It would also be valuable to extend our work to explore competing orders in models which spontaneously break these symmetries [11,12] and study the impact of charge doping [30]. Finally, our work lends impetus to extend the exploration of kagome skyrmion materials [36] to the quantum regime to study the melting of skyrmion crystals as a route to CSLs.

Acknowledgments. We acknowledge funding from the Natural Sciences and Engineering Research Council of Canada through Discovery Grants (No. RGPIN-2021-03214 and No. RGPIN-2017-05759), and computational resources provided by Sharcnet [66] and the Digital Research Alliance of Canada [67].

A.B. and A.H. contributed equally to this paper.

[1] L. Balents, Spin liquids in frustrated magnets, Nature (London) **464**, 199 (2010).

[2] T. Grover, Y. Zhang, and A. Vishwanath, Entanglement entropy as a portal to the physics of quantum spin liquids, New J. Phys. **15**, 025002 (2013).

[3] L. Savary and L. Balents, Quantum spin liquids: A review, Rep. Prog. Phys. **80**, 016502 (2017).

[4] J. R. Chamorro, T. M. McQueen, and T. T. Tran, Chemistry of quantum spin liquids, Chem. Rev. **121**, 2898 (2021).

[5] V. Kalmeyer and R. B. Laughlin, Equivalence of the Resonating-Valence-Bond and Fractional Quantum Hall States, Phys. Rev. Lett. **59**, 2095 (1987).

[6] D. F. Schroeter, E. Kapit, R. Thomale, and M. Greiter, Spin Hamiltonian for which the Chiral Spin Liquid is the Exact Ground State, Phys. Rev. Lett. **99**, 097202 (2007).

[7] H. Yao and S. A. Kivelson, Exact Chiral Spin Liquid with Non-Abelian Anyons, Phys. Rev. Lett. **99**, 247203 (2007).

[8] R. Thomale, E. Kapit, D. F. Schroeter, and M. Greiter, Parent Hamiltonian for the chiral spin liquid, Phys. Rev. B **80**, 104406 (2009).

[9] L. Cincio and G. Vidal, Characterizing Topological Order by Studying the Ground States on an Infinite Cylinder, Phys. Rev. Lett. **110**, 067208 (2013).

[10] B. Bauer, L. Cincio, B. P. Keller, M. Dolfi, G. Vidal, S. Trebst, and A. W. W. Ludwig, Chiral spin liquid and emergent anyons in a kagome lattice Mott insulator, Nat. Commun. **5**, 5137 (2014).

[11] Y.-C. He, D. N. Sheng, and Y. Chen, Chiral Spin Liquid in a Frustrated Anisotropic Kagome Heisenberg Model, Phys. Rev. Lett. **112**, 137202 (2014).

[12] S.-S. Gong, W. Zhu, L. Balents, and D. N. Sheng, Global phase diagram of competing ordered and quantum spin-liquid phases on the kagome lattice, Phys. Rev. B **91**, 075112 (2015).

[13] A. Wietek, A. Sterdyniak, and A. M. Läuchli, Nature of chiral spin liquids on the kagome lattice, Phys. Rev. B **92**, 125122 (2015).

[14] Y.-C. He, S. Bhattacharjee, F. Pollmann, and R. Moessner, Kagome Chiral Spin Liquid as a Gauged U(1) Symmetry Protected Topological Phase, Phys. Rev. Lett. **115**, 267209 (2015).

[15] A. Wietek and A. M. Läuchli, Chiral spin liquid and quantum criticality in extended $s = \frac{1}{2}$ Heisenberg models on the triangular lattice, Phys. Rev. B **95**, 035141 (2017).

[16] A. Szasz, J. Motruk, M. P. Zaletel, and J. E. Moore, Chiral Spin Liquid Phase of the Triangular Lattice Hubbard Model: A Density Matrix Renormalization Group Study, Phys. Rev. X **10**, 021042 (2020).

[17] C. Hickey, L. Cincio, Z. Papić, and A. Paramekanti, Haldane-Hubbard Mott Insulator: From Tetrahedral Spin Crystal to Chiral Spin Liquid, Phys. Rev. Lett. **116**, 137202 (2016).

[18] M. Mekata, Kagome: The story of the basketweave lattice, Phys. Today **56**(2), 12 (2003).

[19] M. B. Hastings, Dirac structure, RVB, and goldstone modes in the kagomé antiferromagnet, Phys. Rev. B **63**, 014413 (2000).

[20] Y. Ran, M. Hermele, P. A. Lee, and X.-G. Wen, Projected-wave-function study of the spin-$\frac{1}{2}$ Heisenberg model on the kagomé lattice, Phys. Rev. Lett. **98**, 117205 (2007).

[21] Y. Iqbal, F. Becca, and D. Poilblanc, Projected wave function study of $\mathbb{Z}_2$ spin liquids on the kagome lattice for the spin-$\frac{1}{2}$ quantum Heisenberg antiferromagnet, Phys. Rev. B **84**, 020407 (2011).

[22] Y.-C. He, M. P. Zaletel, M. Oshikawa, and F. Pollmann, Signatures of Dirac Cones in a DMRG Study of the Kagome Heisenberg Model, Phys. Rev. X **7**, 031020 (2017).

[23] Y. Iqbal, F. Ferrari, A. Chauhan, A. Parola, D. Poilblanc, and F. Becca, Gutzwiller projected states for the $J_1 - J_2$ Heisenberg model on the kagome lattice: Achievements and pitfalls, Phys. Rev. B **104**, 144406 (2021).

[24] L. Messio, B. Bernu, and C. Lhuillier, Kagome Antiferromagnet: A Chiral Topological Spin Liquid? Phys. Rev. Lett. **108**, 207204 (2012).

[25] J. S. Helton, K. Matan, M. P. Shores, E. A. Nytko, B. M. Bartlett, Y. Yoshida, Y. Takano, A. Suslov, Y. Qiu, J.-H. Chung *et al.*, Spin Dynamics of the Spin-$\frac{1}{2}$ Kagome Lattice Antiferromagnet $ZnCu_3(OH)_6Cl_2$, Phys. Rev. Lett. **98**, 107204 (2007).

[26] P. Khuntia, M. Velazquez, Q. Barthélemy, F. Bert, E. Kermarrec, A. Legros, B. Bernu, L. Messio, A. Zorko, and P. Mendels, Gapless ground state in the archetypal quantum kagome antiferromagnet $ZnCu_3(OH)_6Cl_2$, Nat. Phys. **16**, 469 (2020).

[27] R. W. Smaha, W. He, J. M. Jiang, J. Wen, Y.-F. Jiang, J. P. Sheckelton, C. J. Titus, S. G. Wang, Y.-S. Chen, S. J. Teat *et al.*, Materializing rival ground states in the barlowite family of kagome magnets: Quantum spin liquid, spin ordered, and valence bond crystal states, npj Quantum Mater. **5**, 23 (2020).

[28] M. Claassen, H.-C. Jiang, B. Moritz, and T. P. Devereaux, Dynamical time-reversal symmetry breaking and photo-induced chiral spin liquids in frustrated Mott insulators, Nat. Commun. **8**, 1192 (2017).

[29] Y.-H. Zhang, D. N. Sheng, and A. Vishwanath, SU(4) Chiral Spin Liquid, Exciton Supersolid, and Electric Detection in Moiré Bilayers, Phys. Rev. Lett. **127**, 247701 (2021).

[30] Y.-F. Jiang and H.-C. Jiang, Topological Superconductivity in the Doped Chiral Spin Liquid on the Triangular Lattice, Phys. Rev. Lett. **125**, 157002 (2020).

[31] X.-Y. Song, A. Vishwanath, and Y.-H. Zhang, Doping the chiral spin liquid: Topological superconductor or chiral metal, Phys. Rev. B **103**, 165138 (2021).

[32] G. Semeghini, H. Levine, A. Keesling, S. Ebadi, T. T. Wang, D. Bluvstein, R. Verresen, H. Pichler, M. Kalinowski, R. Samajdar *et al.*, Probing topological spin liquids on a programmable quantum simulator, Science **374**, 1242 (2021).

[33] N. Nagaosa and Y. Tokura, Topological properties and dynamics of magnetic skyrmions, Nat. Nanotechnol. **8**, 899 (2013).

[34] A. Fert, N. Reyren, and V. Cros, Magnetic skyrmions: advances in physics and potential applications, Nat. Rev. Mater. **2**, 17031 (2017).

[35] T. Kurumaji, T. Nakajima, M. Hirschberger, A. Kikkawa, Y. Yamasaki, H. Sagayama, H. Nakao, Y. Taguchi, T.-H. Arima, and Y. Tokura, Skyrmion lattice with a giant topological hall effect in a frustrated triangular-lattice magnet, Science **365**, 914 (2019).

[36] M. Hirschberger, T. Nakajima, S. Gao, L. Peng, A. Kikkawa, T. Kurumaji, M. Kriener, Y. Yamasaki, H. Sagayama, H. Nakao *et al.*, Skyrmion phase and competing magnetic orders on a breathing kagomé lattice, Nat. Commun. **10**, 5831 (2019).

[37] S. Hayami, T. Okubo, and Y. Motome, Phase shift in skyrmion crystals, Nat. Commun. **12**, 6927 (2021).

[38] W. Wang, D. Song, W. Wei, P. Nan, S. Zhang, B. Ge, M. Tian, J. Zang, and H. Du, Electrical manipulation of skyrmions in a chiral magnet, Nat. Commun. **13**, 1593 (2022).

[39] B. R. Ortiz, L. C. Gomes, J. R. Morey, M. Winiarski, M. Bordelon, J. S. Mangum, I. W. H. Oswald, J. A. Rodriguez-Rivera, J. R. Neilson, S. D. Wilson *et al.*, New kagome prototype materials: Discovery of KV_3Sb_5, RbV_3Sb_5, and CsV_3Sb_5, Phys. Rev. Mater. **3**, 094407 (2019).

[40] H. Zhao, H. Li, B. R. Ortiz, S. M. L. Teicher, T. Park, M. Ye, Z. Wang, L. Balents, S. D. Wilson, and I. Zeljkovic, Cascade of correlated electron states in the kagome superconductor CsV_3Sb_5, Nature (London) **599**, 216 (2021).

[41] Y.-X. Jiang, J.-X. Yin, M. M. Denner, N. Shumiya, B. R. Ortiz, G. Xu, Z. Guguchia, J. He, M. S. Hossain, X. Liu *et al.*, Unconventional chiral charge order in kagome superconductor KV_3Sb_5, Nat. Mater. **20**, 1353 (2021).

[42] R. Khasanov, D. Das, R. Gupta, C. Mielke, M. Elender, Q. Yin, Z. Tu, C. Gong, H. Lei, E. Ritz *et al.*, Charge order breaks time-reversal symmetry in CsV_3Sb_5, Phys. Rev. Res. **4**, 023244 (2022).

[43] T. Neupert, M. M. Denner, J.-X. Yin, R. Thomale, and M. Z. Hasan, Charge order and superconductivity in kagome materials, Nat. Phys. **18**, 137 (2022).

[44] X. Teng, L. Chen, F. Ye, E. Rosenberg, Z. Liu, J.-X. Yin, Y.-X. Jiang, J. S. Oh, M. Z. Hasan, K. J. Neubauer *et al.*, Discovery of charge density wave in a correlated kagome lattice antiferromagnet, Nature **609**, 490 (2022).

[45] S. Kivelson, C. Kallin, D. P. Arovas, and J. R. Schrieffer, Cooperative ring exchange and the fractional quantum hall effect, Phys. Rev. B **36**, 1620 (1987).

[46] A. V. Chubukov, S. Sachdev, and T. Senthil, Quantum phase transitions in frustrated quantum antiferromagnets, Nucl. Phys. B **426**, 601 (1994).

[47] C. Hickey, L. Cincio, Z. Papić, and A. Paramekanti, Emergence of chiral spin liquids via quantum melting of noncoplanar magnetic orders, Phys. Rev. B **96**, 115115 (2017).

[48] F. Oliviero, J. A. Sobral, E. C. Andrade, and R. G. Pereira, Noncoplanar magnetic orders and gapless chiral spin liquid on the kagome lattice with staggered scalar spin chirality, SciPost Phys. **13**, 050 (2022).

[49] X. G. Wen, F. Wilczek, and A. Zee, Chiral spin states and superconductivity, Phys. Rev. B **39**, 11413 (1989).

[50] E. Fradkin and F. A. Schaposnik, Chern-Simons Gauge Theories, Confinement, and the Chiral Spin Liquid, Phys. Rev. Lett. **66**, 276 (1991).

[51] Q. Zhang and T. Li, Bosonic resonating valence bond theory of the possible chiral spin-liquid state in the triangular-lattice Hubbard model, Phys. Rev. B **104**, 075103 (2021).

[52] J. Pitts, F. L. Buessen, R. Moessner, S. Trebst, and K. Shtengel, Order by disorder in classical kagome antiferromagnets with chiral interactions, Phys. Rev. Res. **4**, 043019 (2022).

[53] See Supplemental Material at http://link.aps.org/supplemental/10.1103/PhysRevB.107.L020411 for details of (i) linear SWT including extrapolation of correlations to the thermodynamic limit, (ii) parton mean-field theory, (iii) variational quantum Monte Carlo study, and (iv) exact diagonalization calculations with additional results.

[54] L. Messio, C. Lhuillier, and G. Misguich, Lattice symmetries and regular magnetic orders in classical frustrated antiferromagnets, Phys. Rev. B **83**, 184401 (2011).

[55] H. Watanabe, Counting rules of nambu goldstone modes, Annu. Rev. Condens. Matter Phys. **11**, 169 (2020).

[56] J. B. Marston and C. Zeng, Spin-peierls and spin-liquid phases of kagomé quantum antiferromagnets, J. Appl. Phys. **69**, 5962 (1991).

[57] T. Fukui, Y. Hatsugai, and H. Suzuki, Chern numbers in a discretized Brillouin zone: Efficient method to compute (spin) Hall conductances, J. Phys. Soc. Jpn. **74**, 1674 (2005).

[58] W.-J. Hu, W. Zhu, Y. Zhang, S. Gong, F. Becca, and D. N. Sheng, Variational Monte Carlo study of a chiral spin liquid in the extended Heisenberg model on the kagome lattice, Phys. Rev. B **91**, 041124(R) (2015).

[59] R. Haghshenas, S.-S. Gong, and D. N. Sheng, Single-layer tensor network study of the Heisenberg model with chiral interactions on a kagome lattice, Phys. Rev. B **99**, 174423 (2019).

[60] P. W. Leung and V. Elser, Numerical studies of a 36-site kagome antiferromagnet, Phys. Rev. B **47**, 5459 (1993).

[61] C. Waldtmann, H. U. Everts, B. Bernu, C. Lhuillier, P. Sindzingre, P. Lecheminant, and L. Pierre, First excitations of the spin $\frac{1}{2}$ Heisenberg antiferromagnet on the kagomé lattice, Eur. Phys. J. B **2**, 501 (1998).

[62] A. M. Läuchli, J. Sudan, and R. Moessner, $s = \frac{1}{2}$ kagome Heisenberg antiferromagnet revisited, Phys. Rev. B **100**, 155142 (2019).

[63] A. M. Läuchli, J. Sudan, and E. S. Sørensen, Ground-state energy and spin gap of spin-$\frac{1}{2}$ kagomé-Heisenberg antiferromagnetic clusters: Large-scale exact diagonalization results, Phys. Rev. B **83**, 212401 (2011).

[64] Since the two lowest $S^z_T = 0$ states are not degenerate with any $S^z_T = 1$ state, they are clearly both spin singlets with total spin $S = 0$. Likewise, the lowest $S^z_T = 1$ state must be a triplet with total spin $S = 1$ since it is not degenerate with any $S^z_T = 2$ state.

[65] A. F. Albuquerque, F. Alet, C. Sire, and S. Capponi, Quantum critical scaling of fidelity susceptibility, Phys. Rev. B **81**, 064418 (2010).

[66] http://www.sharcnet.ca.

[67] https://alliancecan.ca.